INL/JOU-17-40948-Revision-0

Elevated temperature for life extension of lithium ion power cells

Tanvir R Tanim, Mayank Garg, Christopher D. Rahn, Niklas Legnedahl, Hanna Bryngelsson

June 2018

The INL is a U.S. Department of Energy National Laboratory
operated by Battelle Energy Alliance

INL/JOU-17-40948-Revision-0

Elevated temperature for life extension of lithium ion power cells

Tanvir R Tanim, Mayank Garg, Christopher D. Rahn, Niklas Legnedahl, Hanna Bryngelsson

June 2018

Idaho National Laboratory
Idaho Falls, Idaho 83415

http://www.inl.gov

Prepared for the
U.S. Department of Energy
Office of Nuclear Energy
Under DOE Idaho Operations Office
Contract Unknown

Elevated temperature for life extension of lithium ion power cells

Mayank Garg[a,1,*], Tanvir R. Tanim[b,2], Christopher D. Rahn[a,3,**], Hanna Bryngelsson[c,4], Niklas Legnedahl[c,4]

[a] *Department of Mechanical and Nuclear Engineering, The Pennsylvania State University, University Park, Pennsylvania 16802.*
[b] *Energy Storage and Advanced Vehicles,Idaho National Laboratory , Idaho Falls, Idaho*
[c] *Volvo Group Trucks Technology, Gothenburg, Sweden*

Abstract

Lithium ion (Li-ion) cells are increasingly being used in high power applications such as Hybrid Electric Vehicles. This paper investigates how the life of lithium ion power cells can be increased by increasing their temperature. End of life (EOL) in power applications is often defined as when the battery is no longer able to provide the required charge/discharge power because the battery voltage exceeds the maximum/minimum allowable voltages associated with the battery's chemistry. This paper shows that battery life can be increased by step-wise temperature increases whenever the battery voltage exceeds a voltage limit when the EOL is reached. Experiments are conducted on commercially available lithium iron phosphate batteries for six months using a charge sustaining HEV cycle. Two, 1° C temperature increases extend the life of the cells by 2000 cycles (3 months of continuous cycling).

Keywords: Lithium ion battery, Battery management system, Hybrid electric vehicle, Battery aging model

*Corresponding author
**Principal corresponding author
Email addresses: mxg10420@psu.edu (Mayank Garg), tanvir.tanim@inl.gov (Tanvir R. Tanim), cdrahn@psu.edu (Christopher D. Rahn)
[1] Graduate research assistant
[2] Battery R&D Scientist,Idaho National Laboratory
[3] Professor and Co-director of the Battery and Energy Storage Technology Center
[4] Energy storage system specialists, GSR-Energy Storage System

1. Introduction

Li-ion batteries have diverse applications such as portable electronics, energy storage, Hybrid Electric Vehicles (HEVs), plug-in HEVs, and electric vehicles (EVs). High energy density and longer life are major reasons for the widespread use of lithium ion batteries. Presently, almost all major automobile manufacturers have hybrid vehicles in the market. HEVs can also help to reduce greenhouse gases and improve power train efficiency [1].

HEV batteries are typically sized to meet power (rather than energy storage) requirements. Lithium iron phosphate (LFP) batteries are popular power cells with a highly stable cathode due to its olivine crystal structure. A major degradation mechanism in LFP batteries is solid electrolyte interphase (SEI) layer growth on the graphite negative electrode, that leads to the loss of the active material and capacity [2, 3, 4]. Safari *et al.* [5] experimentally showed that SEI layer growth is affected by usage and operating temperature. Ramadass *et al.* [6] proposed a simplified, control-oriented SEI growth model. Randall *et al.* [7] simplified this model and proposed an iterative approach to calculate the SEI side reaction current density. Tanim *et al.* [8] further simplified the aging model to develop analytical formulas for capacity fade and impedance rise.

Modern battery management systems (BMS) require fast and accurate battery models to resolve the control, management and estimation tasks in real time. Equivalent circuit models (ECMs) are argued to be more suitable in implementing BMS algorithms due to their simple format and computationally less expensive nature [9, 10, 11, 12]. The states of ECMs are, however, disconnected from the underlying physical mechanisms. ECMs also require extensive experimental data to empirically tune for each temperature, state of charge (SOC), and state of health (SOH). Alternatively, reduced-order, control-oriented, physics-based models can be sufficiently accurate and fast [13, 14, 15, 16, 17, 18]. Prasad *et al.* [13] developed a linear single particle, performance model that could be realized as an equivalent circuit, unifying these two approaches. Tanim *et al.*

[14] also developed a seventh order electrolyte Enhanced Single Particle Model (ESPM) by adding electrolyte dynamics to the single particle model. The addition of electrolyte dynamics in Tanim's model has improved the voltage estimation of the power cell for charge-discharge pulses up to 25C rate.

According to the U.S. Advanced Battery Consortium (USABC), battery EOL in EV applications is reached when battery remaining capacity or peak power decreases to 80% of the rated value [19]. The USABC definition of EOL may not be suitable for HEVs. HEVs operate on charge sustaining cycles in small SOC windows to provide the required power without exceeding pre-defined voltage limits. An alternative EOL definition for HEVs is proposed in FreedomCAR Battery Test Manual [20] as follows: A battery pack is at EOL when the voltage first exceeds a maximum/minimum voltage limit during normal operation and the test profile cannot be executed within the voltage limits. The maximum allowable voltage is determined by the battery chemistry and manufacturer to maintain safe and long-life operation. This EOL definition is not explicitly based on SOH. HEV batteries can be designed to provide the required pulse power after 80% SOH. EOL implicitly depends on SOH, however, and the impedance rise associated with aging. Normal operation is defined by reasonable charge/discharge current inputs that are represented by a charge-sustaining duty cycle associated with typical HEV operation. Finally, it is typically charge acceptance during breaking that is most likely to result in exceeding a voltage limit so the maximum voltage limit often dictates EOL.

This paper proves the hypothesis that HEV EOL and battery life can be extended by judiciously increasing the battery temperature. Increased battery temperature reduces cell impedance but increases degradation. For power applications, exceeding voltage limits depends on both capacity and impedance of the aged cells. If the decrease in capacity can be overcome by the decrease in impedance, the raising temperature can increase life. HEV battery pack often have thermal management system so raising the temperature may simply entail changing set point in the controller. According to this hypothesis, the battery is operated at its normal temperature until EOL. Then the battery temperature

is increased to reduce impedance and allow cycling without exceeding voltage limits, thus prolonging EOL. Higher battery temperature increases the battery degradation rate [21], however, so the battery capacity and impedance degrade at the accelerated rate until the battery exceeds voltage limit once again. The process of increasing battery temperature in response to exceeded voltage limits can be continued to provide more cycles. Eventually, the battery temperature will reach the safety limit and the battery will truly be dead. This paper is the first to put forth the counter intuitive hypothesis that heating an HEV battery can extend its life. The hypothesis is theoretically and experimentally proven for LFP batteries.

The proposed approach is most effective for power-intensive applications like HEVs because the reduction of impedance caused by controlled temperature rise can directly impact performance in these applications. HEVs typically operate in a broad range of temperatures. It is reasonable to expect that the battery pack will be at or below 35° C a significant amount of time. Thus, it makes sense to consider elevating the pack temperature above 25° C to extend its life. Of course, the pack temperature may be elevated in warm climates without heating. In that case, the proposed approach is not applicable.

It is common to warm up the lithium-ion battery pack from sub-zero temperatures to normal operating temperature (25° C) in HEVs to access the full battery utilization window (e.g., high rate charge-discharge pulses required in HEVs) efficiently and eliminate any concern of lithium plating. Thus, life extension of a battery pack by increasing temperature for sub-zero extreme temperature applications is not relevant from the practical point of view concerning the performance and safety of the lithium-ion battery.

2. MATHEMATICAL MODELING

Figure 1 shows a schematic diagram of the pseudo-2D Li-ion battery model [22, 23, 24, 25] that is the basis of the theoretical study. The current input I(t) charges (I>0) and discharges (I<0) the cell to produce the output voltage V(t).

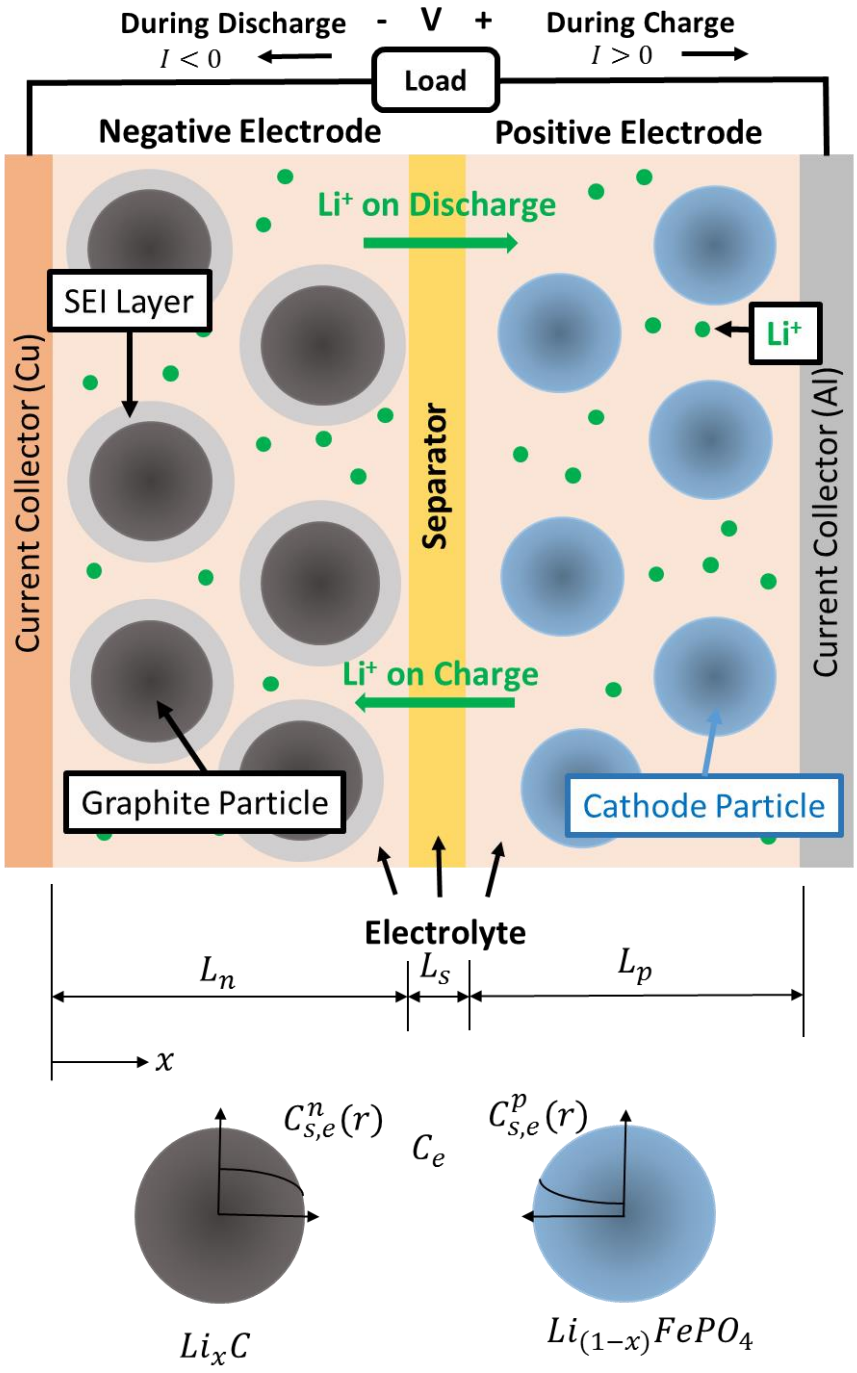

Figure 1: **Schematic diagram of a pseudo-2D Li-ion cell model.**

Lithium ions shuttle back and forth between the negative electrode ($x < L_n$) and positive electrode ($L_n + L_s < x < L_n + L_s + L_p$) through the separator ($L_n < x < L_n + L_s$). The model variables include solid phase concentration c_s in the active material particles, electric potential ϕ in the solid (s) and electrolyte (e) phases, electrolyte phase concentration c_e, and exchange current density j^{Li} and over-potential η in the two electrodes. Table 1 lists the governing equations of the ESPM, reduced order model developed in [14].

The following assumptions apply to the ESPM model:

1. The ESPM assumes that j^{Li} is uniform (infinite electrode conductivity) across each electrode so all material particles are in parallel and the solid phase of each electrode can be represented by a single, spherical material particle.
2. The battery temperature T is assumed to be fixed and uniform.
3. The ESPM is linearized around a fixed SOC set point.

These assumptions reduce the full-order model to the simplified transfer functions given in Table 2. The solid phase Li-ion diffusion Eq. (1) is solved using Laplace transformation and Padé approximation resulting in the transfer functions for the positive and negative particles in Eqs. (8a) and (8b). Equation 2 governs the solid phase charge conservation and reduces to uniform current distributions within the two electrodes in the Eqs. (9a) and (9b). Equation (3) and (4) govern the electrolyte dynamics and are simplified using a third order Integral Method Approximation to obtain the second order transfer function in Eq. (10). The Butler-Volmer (B-V) relating current density and overpotential is linearized in Eq. (11a) and (11b). The overpotential at the particle surface in Eq. (6) and output voltage Eq. (7) become Eq. (12) in the ESPM. The parameters for the ESPM model of the LFP cells are given in Table 3.

Increase temperature can accelerate aging so the ESPM is augmented with an SEI layer growth model that incorporates a predominant aging mechanism for LFP cells. The SEI layer forms on the graphite particle in the anode, consumes active lithium material, and reduces the battery capacity. A control oriented

SEI layer degradation model is developed by Tanim *et al.* [8] which is based on the previous work of Ramadass *et al.* [6] and Randall *et al.* [7].

The model assumes:

1. The current density of the aging side reaction is much less than the current density of main charge/discharge reaction.
2. The resistance growth due to SEI layer formation is negligible.

The governing equations for calculating the capacity fade are given in Table 4. The side reaction current density j_n^{sei} is related through Tafel kinetics to the side reaction overpotential η_{sei}. The overpotential depends on the fields in the negative electrode ϕ_s^n and the electrolyte ϕ_e calculated from the performance model. Side reaction equilibrium potential, U_{sei}^{ref} is 0.4 V. The capacity loss Q_{loss} is proportional to the time integration of j_n^{sei}. The aging model has been previously validated for LFP cells at 33° C cell surface temperature [8]. In this paper, the model is further validated at higher temperatures, different initial SOHs, and wider ranges of SOH.

3. EXPERIMENTAL SETUP

Figure 2(a) shows the experimental set up used to validate the proposed models and provide evidence that supports the hypothesis. Six LFP cells with different initial SOHs are aged in two different experiments. In both experiments, a pack comprising three commercially available 4.5 Ah cylindrical graphite/LFP cells connected in parallel is placed in the temperature controlled environmental chamber. The packs are cycled using a HEV profile with an Arbin BT-2000. The three cells have the same voltage. The current of the individual cells is measured using Hall Effect current sensors. Cell capacity is measured at specific intervals in four steps: (1) Charging to 3.6 V at 1C constant current; (2) Holding voltage constant at 3.6 V until the current drop to C/20; (3) Resting for 30 min; and (4) Discharging at 1C rate to a cut-off voltage of 2.0 V.

Table 1: ESPM Model Equations [14]

Reaction	**Equation**	**Boundary conditions**	
Solid phase Li^+ conservation	$\frac{\partial c_s}{\partial t} = \frac{D_s}{r^2}\frac{\partial}{\partial r}\left(r^2\frac{\partial c_s}{\partial r}\right)$	$\left.\frac{\partial c_s}{\partial x}\right\|_{r=0} = 0, -D_s\left.\frac{\partial c_s}{\partial x}\right\|_{r=R_s} = \frac{j^{Li}}{a_s F}$	(1)
Solid phase charge conservation	$\frac{\partial}{\partial x}\left(\sigma^{eff}\frac{\partial}{\partial x}\phi_s\right) = j^{Li}$	$-\sigma^{eff}\left.\frac{\partial \phi_s}{\partial x}\right\|_{x=0} = \sigma^{eff}\left.\frac{\partial \phi_s}{\partial x}\right\|_{x=L} = \frac{I}{A}$, $\left.\frac{\partial \phi_s}{\partial x}\right\|_{x=L_n} = \left.\frac{\partial \phi_s}{\partial x}\right\|_{x=L_n+L_s} = 0$	(2)
Electrolyte phase Li^+ conservation	$\frac{\partial(\epsilon_e c_e)}{\partial t} = \frac{\partial}{\partial x}\left(D_e^{eff}\frac{\partial}{\partial x}c_e\right) + \frac{1-t_+^0}{F}j^{Li}$	$\left.\frac{\partial c_e}{\partial x}\right\|_{x=0} = \left.\frac{\partial c_e}{\partial x}\right\|_{x=L} = 0$	(3)
Electrolyte phase charge conservation	$\frac{\partial}{\partial x}\left(k^{eff}\frac{\partial}{\partial x}\phi_e\right) + \frac{\partial}{\partial x}\left(k_D^{eff}\frac{\partial}{\partial x}\ln c_e\right) + j^{Li} = 0$	$\left.\frac{\partial \phi_e}{\partial x}\right\|_{x=0} = \left.\frac{\partial \phi_e}{\partial x}\right\|_{x=L} = 0$	(4)
Butler-Volmer Equation	$j^{Li} = a_s i_0\left[exp\left(\frac{\alpha_a F}{RT}\eta\right) - exp\left(-\frac{\alpha_c F}{RT}\eta\right)\right]$		(5)
Overpotential Equation	$\eta = \phi_s - \phi_e - U$		(6)
Voltage Output Equation	$V(t) = \phi_s(L,t) - \phi_s(0,t) - \frac{R_c}{A}I(t)$		(7)

Table 2: Reduced order ESPM Model [14]

Reaction	**Transfer function**	
Solid phase Li^+ conservation		
Positive particle	$\frac{\tilde{C}^p_{s,e}}{I(s)} = \frac{21\left(\frac{s^2}{a^p_s F A_p R^p_s L_p} + \frac{60 D^p_s s}{a^p_s F A_p [R^p_s]^3 L_p} + \frac{495[D^p_s]^2}{a^p_s F A_p [R^p_s]^5 L_p}\right)}{s^3 + \frac{189 D^p_s s^2}{[R^p_s]^2} + \frac{3465[D^p_s]^2 s}{[R^p_s]^4}}$	(8a)
Negative particle	$\frac{\tilde{C}^n_{s,e}}{I(s)} = \frac{-21\left(\frac{s^2}{a^n_s F A_n R^n_s L_n} + \frac{60 D^n_s s}{a^n_s F A_n [R^n_s]^3 L_n} + \frac{495[D^n_s]^2}{a^n_s F A_n [R^n_s]^5 L_n}\right)}{s^3 + \frac{189 D^n_s s^2}{[R^n_s]^2} + \frac{3465[D^n_s]^2 s}{[R^n_s]^4}}$	(8b)
Solid phase charge conservation		
Positive particle	$\frac{J^L_p i}{I(s)} = -\frac{1}{A_p L_p}$	(9a)
Negative particle	$\frac{J^L_n i}{I(s)} = \frac{1}{A_n L_n}$	(9b)
Electrolyte phase Li^+ and charge conservation	$\frac{\Delta\phi_e(L,s)}{I(s)} = \frac{-0.000865 s^2 - 0.0010 s - 0.00025}{s^2 + 0.9501 s + 0.1024}$	(10)
Butler-Volmer Equation		
Positive particle	$\frac{\eta_p(s)}{I(s)} = -\frac{R^p_{ct}}{a^p_s}\frac{1}{A_p L_p};\ R^p_{ct} = \frac{RT}{F(\alpha_a + \alpha_c) i_0}\ ;\ a^p_s = \frac{3\varepsilon^p_s}{R^p_s}$	(11a)
Negative particle	$\frac{\eta_n(s)}{I(s)} = \frac{R^n_{ct}}{a^n_s}\frac{1}{A_n L_n};\ R^n_{ct} = \frac{RT}{F(\alpha_a + \alpha_c) i_0}\ ;\ a^n_s = \frac{3\varepsilon^n_s}{R^n_s}$	(11b)
Voltage Output Equation	$\frac{\widetilde{V}(s)}{I(s)} = \frac{\eta_p(s)}{I(s)} + \frac{\partial U}{\partial \tilde{C}^p_{s,e}}\frac{\tilde{C}^p_{s,e}}{I(s)} - \frac{\eta_n(s)}{I(s)} - \frac{\partial U}{\partial \tilde{C}^n_{s,e}}\frac{\tilde{C}^n_{s,e}}{I(s)} + \frac{\Delta\phi_e(L,s)}{I(s)} - \frac{R_c}{A}$	(12)

Table 3: Model parameters of a 4.5 Ah LFP cell[8]

Parameter	**Neg. electrode**	**Pos. electrode**
Thickness, L (cm)	3.40×10^{-3}	7.00×10^{-3}
Particle radius, R_s (cm)	2.90×10^{-4}	3.65×10^{-6}
Active material volume fraction, ε_s	0.55	0.41
Exchange current density, $i_{0,ref}$ (A cm^{-2})	1.85×10^{-4}	8.18×10^{-5}
Charge transfer coefficient, α_a, α_c	0.5, 0.5	0.5, 0.5
Solid phase Li diffusion coefficient, $D_{s,ref}$ (cm^2 s^{-1})	5.29×10^{-11}	1.18×10^{-14}
Area, A (cm^2)	3580	3487

Table 4: Governing equations of the SEI growth model [8]

Reaction	**Equation**	
Tafel equation (SEI reaction):	$j_n^{sei} = -a_s^n i_{0,sei} exp\left(-\frac{\alpha_n F}{RT}\eta_{sei}\right)$	(14)
Side reaction overpotential:	$\eta_{sei} = \phi_s^n - \phi_e - U_{sei}^{ref}$	(15)
Capacity loss:	$\frac{\partial Q_{Loss}}{\partial t} = -j_n^{sei} A_n L_n$	(18)

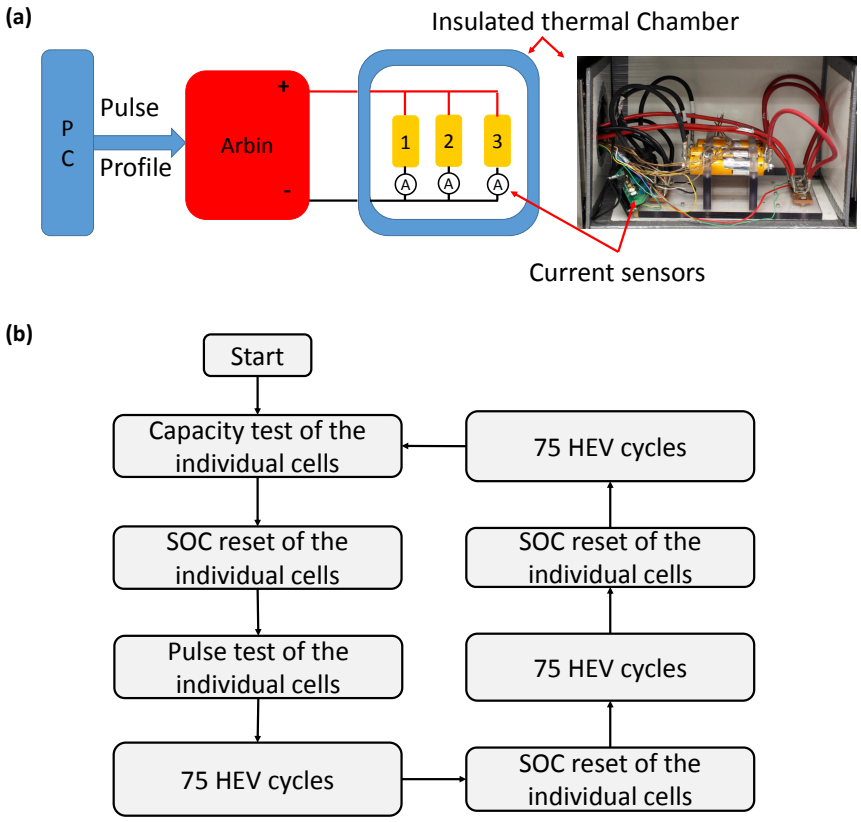

Figure 2: **Experimental testing of LFP battery pack with 3 cells in parallel: (a) Set up, and (b) Procedure.**

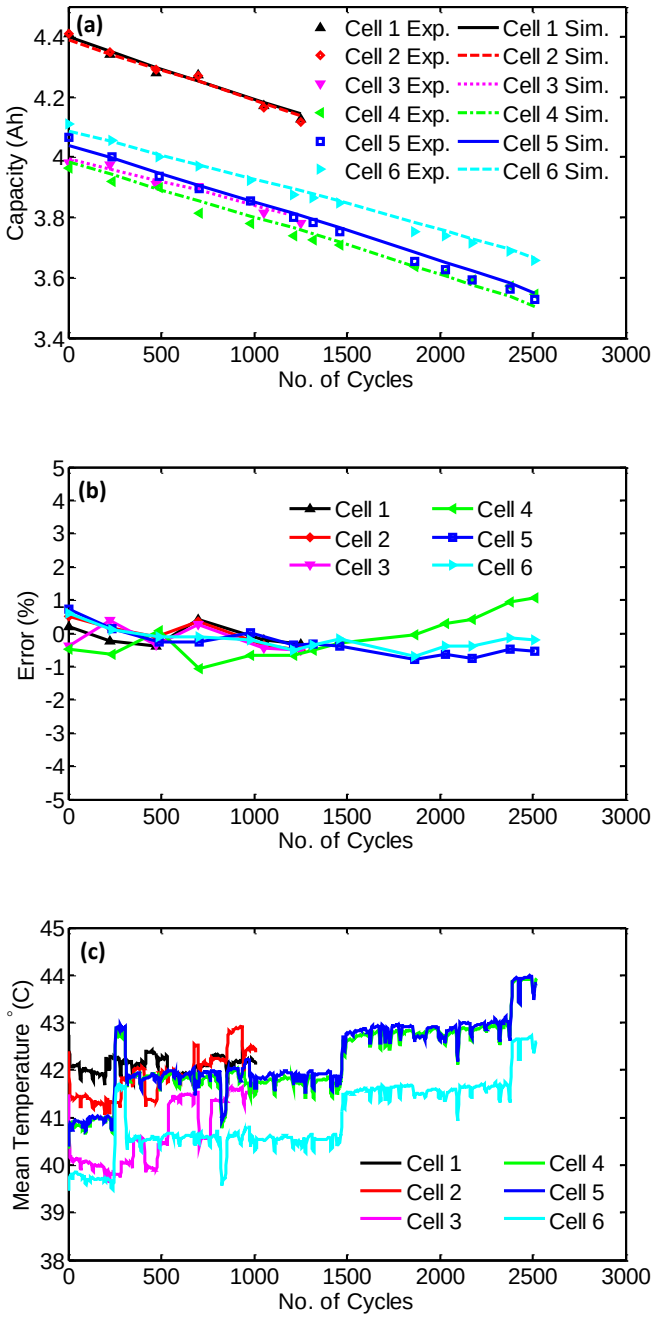

Figure 3: **Experiment 1 cycling results: (a) Theoretical (lines) and experimental (symbols) capacity fade, (b) Model error, and (c) Cell temperature versus number of cycles.**

Experiment 1: Model Validation Cell 1, cell 2, and cell 3 have initial capacities of 4.41 Ah, 4.41 Ah, and 3.98 Ah, respectively. Cell 1 and Cell 2 are fresh cells, and cell 3 is 10% aged from previous experiments and calendar aging. Initial SOC of the cells is 44.55%. The SOC point was selected in a mid-range to provide the maximum discharge pulse and absorb the maximum charge pulse of the selected HEV cycle. This strategy is typically followed in HEV applications. The pack is cycled using a 4200 seconds long charge sustaining HEV cycle that has 10.5 % SOC swing and 182 Amp and -195 Amp maximum and minimum currents, respectively, for 1250 cycles (approximately 3 months) at 37° C environmental chamber temperature.

Experiment 2: Life Extension Cell 4, cell 5, and cell 6 in the second pack have initial capacities of 3.96 Ah, 4.07 Ah, and 4.11 Ah, respectively. All three cells have been aged in other experiments and/or calendar aged. Initial SOC of the cells is 44.55%. In this experiment, the voltage limit corresponding to battery EOL is defined to be 3.571 V and 2.00 V, narrower than required by LFP chemistry to accelerate EOL. The environmental chamber temperature starts at 37° C. The pack is cycled using the SOC resetting protocol in Fig. 2(b) until EOL at 250 cycles. The SOC of individual cells is reset every 4 days (around 75 HEV cycles) to account for the slow SOC drift associated with Arbin current noise. At EOL the pack can no longer provide the required charge acceptance without exceeding the maximum voltage limit. The battery pack temperature is then raised by 1° C and it is once again able to perform the HEV cycle without exceeding the voltage limits. At 1250 cycles, the battery pack again reaches EOL, and its temperature is raised by 1° C so that it cycles further. In this way, chamber temperature is increased up to 40° C with step wise temperature increases of 1° C. Overall, the battery pack undergoes 2500 cycles for approximately 6 months.

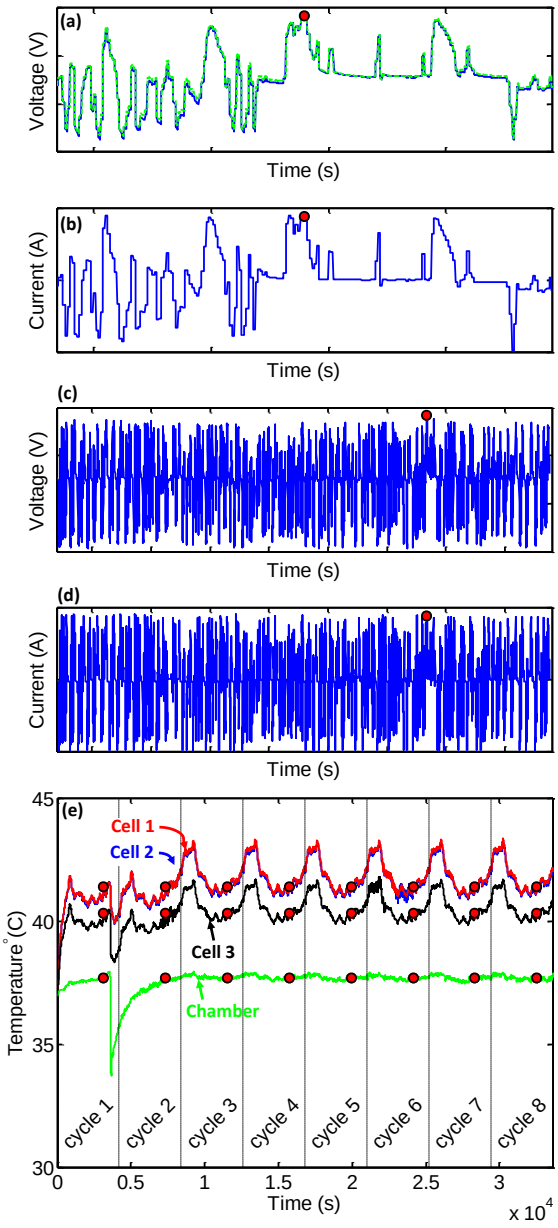

Figure 4: **Experiment 2 cycling results: (a) Theoretical (green-dashed) and experimental (blue-solid) voltage response over 200 seconds of the HEV cycle that includes the maximum voltage (red-dot), (b) Current input corresponding to the voltage response in (a), (c) Voltage response during an entire cycle (d) Current profile of an entire cycle (e) Cell (red, black, blue solid) and chamber (green solid) temperature during 8 cycles.**

4. RESULTS AND DISCUSSION

4.1. Experiment 1: Model Validation

Figure 4(a) shows the voltage time response of a cell to the partial cycle current profile in Fig. 4(b). The model-predicted voltage matches the experimental results within ±0.5%, validating the performance model. Figure 3(a) shows the theoretical and experimental capacity fade results for all six cells. The temperature histories are shown in Figure 3(c) and vary from 39° C to 43° C. The experiment capacity fade and model predictions are shown for different initial SOH and temperature histories. Figure 3(b) shows the capacity fade prediction error is less than ±1% for all 6 cases validating the aging model.

4.2. Experiment 2: Life Extension

Figure 4 shows experimental results from experiment 2. During each cycle there is one point with maximum voltage, typically after long and high current charge pulse as shown in Fig. 4(a) - (d). The minimum voltage is well above the limit. Thus, EOL for this cell, average SOC, and current profile is determined by the charge acceptance/maximum voltage limit. The SOCs of the individual cells drift upward over time and are manually reset every 4 days or roughly 75 HEV cycles. SOC drift causes the battery voltage to increase so only battery voltages shortly after SOC resets are used to determine whether voltage limit has been exceeded. Figure 4(e) shows the temperature profile for the first few HEV cycles after an SOC reset. The environmental chamber and cell temperatures are transient for a few cycles. Temperature also influences voltage so we use the mean of the maximum voltages in HEV cycles 6, 7 and 8 after SOC reset as the V_c to be compared with voltage limits. Figure 4(e) shows the temperature transients in the chamber and cells settling out after 4-5 cycles so cycle 6-8 are at steady state.

Figure 5(b) shows the complete data for experiment 2, consisting of maximum voltage for 2500 HEV cycles. The inset to Fig. 5(a) zooms in to help to explain the effect of the SOC drift on the maximum voltage. The marked points

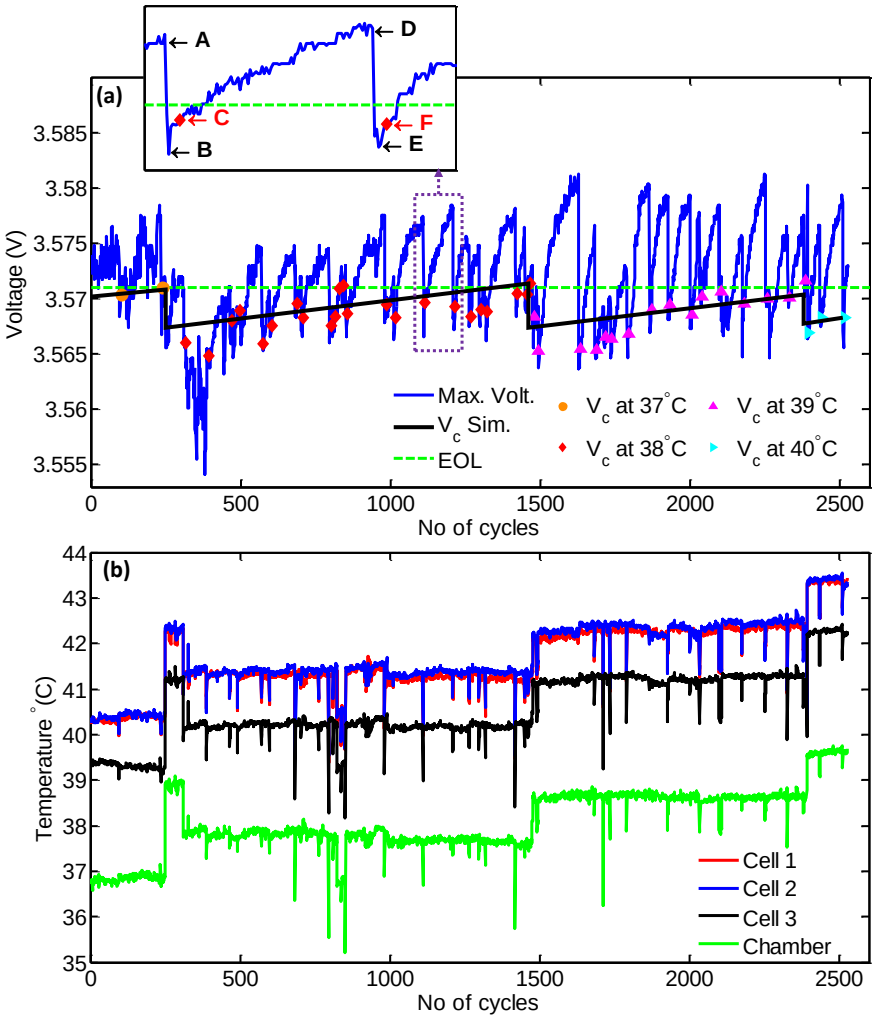

Figure 5: **Experiment 2 cycling results: (a) Maximum voltage in each cycle for 2500 cycles, V_c, the mean of the maximum voltage of cycles 6, 7 and 8 after SOC reset, and EOL is end of life voltage limit; (b) Cell and thermal chamber temperatures.**

in the figure are as follows:

Point A - After every 75 cycles (4 days of aging), the mean SOC has drifted by 4-5%, and the SOC is reset. Point A represents the maximum voltage in the last HEV cycle before SOC of the battery pack was reset.

Point B - Point B is the maximum voltage in the first HEV cycle after the SOC reset. The voltage at point B is lower than the voltage at point A because the SOC at point B is lower than the SOC at point A.

Point C - Point C is at V_c, the average of the maximum voltage in cycles 6, 7 and 8 after the SOC reset.

Points D, E, and F - Points D, E, and F corresponds to points A, B, and C but at the next SOC reset.

Figure 5(b) shows the cell and experimental chamber temperature responses. The cell temperatures track the chamber temperature except a few degree warmer due to internal cell heating. The temperature dropouts/noise are due to start up artifacts.

A 10% aged cell was chosen for experiment 2 and aged for additional 250 cycles at 37° C environmental temperature. After the 250 cycles, V_c was 3.571 V. The maximum voltage limit for a LFP battery is 3.6 V, but 3.571 V is used for EOL in this study. The value of the voltage limit is not critical to demonstrate the effect of increase cell temperatures on voltage response.

After the first 250 cycles, the environmental chamber temperature was increased by 1° C, and the cell surface temperature also increased by around 1° C. Increased cell temperature reduces the effective battery resistance and reduces the maximum voltage in the HEV cycle. The maximum voltage no longer exceeded the EOL, and the battery pack provided more cycles. In the experiment, battery's life was extended by 1250 cycles due to this 1° C temperature increase. After 1250 additional HEV cycles, V_c exceeds the EOL, and the battery pack is no longer able to accept the required charge without exceeding the voltage limit.

Again, the environmental chamber temperature was increased by 1° C to 39° C and the cell surface temperature also increased by 1° C. The battery pack was

able to provide an additional 925 HEV cycles before V_c again exceeded the EOL. After 2425 total cycles, the environmental temperature was again increased by 1° C to show that V_c can be reduced, and the battery's life can be further extended. Figure 5(b) shows decreases in V_c near cycle 250, 1500, and 2425 due to temperature increases and slow increase of V_c from cycle 250 to 1500 and 1500 to 2425 due to capacity fade. Figure 5(b) also shows the model predicted V_c and it matches experimental V_c quite well.

5. CONCLUSION

The paper theoretically and experimentally proves the hypothesis that increasing battery temperature can extend battery life for HEV applications. Two 1° C temperature increases extend the life of a 4.5 Ah LFP cell by 2000 charge sustaining HEV cycles. These small temperature increases allowed the cell to cycle continuously for an additional 3 months.

ACKNOWLEDGMENT

The authors greatly appreciate Volvo Group Trucks Technology for financially supporting this project.

NOMENCLATURE

A	electrode plate area, cm^2
a_s	active surface area per electrode unit volume, cm^2/cm^3
BMS	Battery management system
c	concentration of Li in a phase, mol/cm^3
D	diffusion coefficient of Li, cm^2/s
ECM	Equivalent circuit model
EOL	End of life
EV	Electric vehicles
F	Faraday's constant, 96,487 C/mol

HEV	Hybrid Electric Vehicles
I	applied current, A
i_0	exchange current density of electrode reaction, A/cm^2
j^{Li}	reaction current resulting in production or consumption of Li, A/cm^3
L	cell width, cm
LFP	Lithium Iron Phosphate
$Li-ion$	Lithium ion
Q	capacity, Ah
r	radial coordinate within active material particle, cm
R	universal gas constant, 8.3143 J/mol K
R_c	contact resistance, Ωcm^2
R_s	radius of active material particles, cm
s	Laplace transform variable
SEI	Solid electrolyte interphase
SOC	State of charge
SOH	State of health
T	absolute temperature, K
t	time, s
t_+^0	transference number of Li^+ with respect to solvent velocity
U	open circuit, or equilibrium potential of an electrode reaction, V
V	voltage, V
x	distance, cm

Greek Symbols

α_a, α_c	anodic and cathodic transfer coefficients for an electrode reaction
ε	volume fraction or porosity of a phase
η	overpotential of an electrode reaction, V
κ	Li^+ conductivity of electrolyte, S/cm
κ_D	Li^+ diffusional conductivity of electrolyte, A/cm

σ	e^- conductivity of electrode solid matrix, S/cm
ϕ	phase potential, V

Subscript

e	electrolyte phase
n	negative electrode
p	positive electrode
ref	reference value
s	separator
s, e	solid electrolyte interface
sei	solid electrolyte interface layer

Superscript

eff	effective
Li	Li lithium species
$+$	ion

References

[1] C. D. Rahn, C.-Y. Wang, Battery systems engineering, John Wiley & Sons, 2013.

[2] M. Safari, C. Delacourt, Simulation- based analysis of aging phenomena in a commercial graphite/ lifepo$_4$ cell, J. Electrochem. Soc. 158 (12) (2011) A1436–A1447.

[3] A. Eddahech, O. Briat, J. Vinassa, Performance comparison of four lithium-ion battery technologies under calendar aging, Energy 84 (2015) 542–550.

[4] E. Sarasketa-Zabala, I. Gandiaga, L. Rodriguez-Martinez, I. Villarreal, Calendar aging analysis of a lifepo$_4$/graphite cell with dynamic model validations: Towards realistic lifetime predictions, J. of Power Sources 272 (2014) 45–57.

[5] M. Safari, C. Delacourt, Aging of a commercial graphite/ lifepo$_4$ cell, J. Electrochem. Soc. 158 (10) (2011) A1123–A1135.

[6] P. Ramadass, B. Haran, P. M. Gomadam, R. White, B. N. Popov, Development of first principle capacity fade model for li-ion cells, J. Electrochem. Soc. 151 (2) (2004) A196–A203.

[7] A. V. Randall, R. D. Perkins, X. Zhang, G. L. Plett, Controls oriented reduced order modeling of solid-electrolyte interphase layer growth, Journal of Power Sources 209 (2012) 282–288.

[8] T. R. Tanim, C. D. Rahn, Aging formula for lithium ion batteries with solid electrolyte interphase layer growth, Journal of Power Sources 294 (2015) 239–247.

[9] H. He, X. Zhang, R. Xiong, Y. Xu, H. Guo, Online model-based estimation of state of charge and open circuit voltage of lithium-ion batteries in electric vehicles, Energy 39 (1) (2012) 310–318.

[10] M. W. Verbrugge, R. S. Conell, Electrochemical and thermal characterization of battery modules commensurate with electric vehicle integration, J. Electrochem. Soc. 149 (1) (2002) A45–A53.

[11] M. Verbrugge, P. Liu, Electrochemical characterization of high-power lithium ion batteries using triangular voltage and current excitation sources, J. Power Sources 174 (1) (2007) 2–8.

[12] X. Hu, S. Li, H. Peng, A comparative study of equivalent circuit models for li-ion batteries, Journal of Power Sources 198 (2012) 359–367.

[13] G. K. Prasad, C. D. Rahn, Development of a first principles equivalent circuit model for a lithium ion battery, in: ASME 2012 5th Annual Dynamic Systems and Control Conference joint with the JSME 2012 11th Motion and Vibration Conference, American Society of Mechanical Engineers, 2012, pp. 369–375.

[14] T. R. Tanim, C. D. Rahn, C.-Y. Wang, A temperature dependent, single particle, lithium ion cell model including electrolyte diffusion, Journal of Dynamic Systems, Measurement, and Control 137 (1) (2015) 011005.

[15] T. R. Tanim, C. D. Rahn, C.-Y. Wang, A reduced order electrolyte enhanced single particle lithium ion cell model for hybrid vehicle applications, in: 2014 American Control Conference, IEEE, 2014, pp. 141–146.

[16] T. R. Tanim, C. D. Rahn, C.-Y. Wang, State of charge estimation of a lithium ion cell based on a temperature dependent and electrolyte enhanced single particle model, Energy 80 (2015) 731–739.

[17] K. A. Smith, C. D. Rahn, C.-Y. Wang, Model order reduction of 1d diffusion systems via residue grouping, Journal of Dynamic Systems, Measurement, and Control 130 (1) (2008) 011012.

[18] K. A. Smith, C. D. Rahn, C.-Y. Wang, Model-based electrochemical estimation and constraint management for pulse operation of lithium ion batteries, IEEE Transactions on Control Systems Technology 18 (3) (2010) 654–663.

[19] USABC, Electric vehicle battery test procedures manual, revision 2, southfield, michigan, `https://avt.inl.gov/sites/default/files/pdf/battery/usabc_manual_rev2.pdf`, [United States Advanced Battery Consortium] (1996).

[20] G. Hunt, C. Motloch, Freedom car battery test manual for power-assist hybrid electric vehicles, INEEL, Idaho Falls.

[21] T. R. Tanim, C. D. Rahn, N. Legnedahl, Elevated temperatures can extend the life of lithium iron phosphate cells in hybrid electric vehicles, in: ASME 2015 Dynamic Systems and Control Conference, American Society of Mechanical Engineers, 2015, pp. V002T26A003–V002T26A003.

[22] V. Srinivasan, J. Newman, Discharge model for the lithium iron-phosphate electrode, J. Electrochem. Soc. 151 (2004) A1517–A1529.

[23] M. Doyle, J. Newman, Comparison of modeling predictions with experimental data from plastic lithium ion cells, J. Electrochem. Soc. 143 (6) (1996) 1890–1903.

[24] W. B. Gu, C. Y. Wang, Thermal-electrochemical modeling of battery systems, J. Electrochem. Soc. 147 (8) (2000) 2910–2922.

[25] M. Doyle, Y. Fuentes, Computer simulations of a lithium-ion polymer battery and implications for higher capacity next-generation battery designs, J. Electrochem. Soc. 150 (6) (2003) A706–A713.